

Supporting Information

Strain modulation of Si vacancy emission from SiC micro- and nanoparticles

G. C. Vásquez^{a*}, M. E. Bathen^a, A. Galeckas^a, C. Bazioti^a, K. M. Johansen^a, D. Maestre^b, A. Cremades^b, Ø. Prytz^a, A. M. Moe^c, A. Yu. Kuznetsov^a, L. Vines^a

^a *Centre for Materials Science and Nanotechnology, University of Oslo, N-0318 Oslo, Norway*

^b *Departamento de Física de Materiales, Facultad de CC. Físicas, Universidad Complutense de Madrid, 28040, Madrid, Spain*

^c *Washington Mills AS, NO-7300 Orkanger, Norway*

*Corresponding author

G. Cristian Vasquez

E-mail: g.c.vasquez@smn.uio.no

Contents: Methods, supporting analyses, and additional results and discussion

Supporting Methods

SiC micro- and nanoparticles were provided by Washington Mills Co. Crystals having an average size of 2 and 5 μm were deposited and mechanically dispersed on flat Si substrates. To intentionally create the V_{Si} defects, a sample with SiC particles was irradiated with 1.8 MeV protons to a fluence of $8 \times 10^{13} \text{ cm}^{-2}$ and at an angle 8° off the surface normal to reduce channelling effects. The protons have a projected range of around 27 μm , that is, the Bragg peak of implanted hydrogen is situated far beyond the micron-sized SiC particles. Therefore, we anticipate no involvement of hydrogen in the CL measurements. The irradiation was followed by thermal annealing on a hot plate at 300 $^\circ\text{C}$ for 30 min in air to clear out interstitial defects, similar to that performed in Ref. [7] of the main text.

The samples were studied with a JEOL JSM-IT300 SEM equipped with a Delmic SPARC Cathodoluminescence (CL) System. CL spectra were measured at room temperature (RT) and 80 K with acceleration voltages from 5 to 10 kV and probing currents of 100-200 pA. It is important to mention that the measurements were stable and reproducible, thus the amount of V_{Si} defects studied was not altered by electron irradiation from the SEM. Hyperspectral data was collected with an Andor Shamrock 303i spectrometer with a 300 l/mm grating and a charged couple device (CCD) Andor Newton DU940P-BU2 detector. Long pass filters with cut-off wavelengths of 550 nm were used to block second order diffractions to record the NIR region. Note that the CL spectra have been filtered in order to minimize the etaloning effect caused by optical interference on the back-illuminated CCD detectors in the range 700-1000 nm.

The micro-Raman analysis was performed at room temperature using a Horiba Jobin-Yvon LabRAM HR800 confocal microscope equipped with a 325-nm He-Cd laser source. The laser power density of about $8 \times 10^4 \text{ W} \cdot \text{cm}^{-2}$ was attenuated by using a neutral filter to avoid thermal heating effects.

(Scanning) Transmission Electron Microscopy (S)TEM investigations were conducted on a FEI Titan G2 60-300 kV equipped with a CEOS DCOR probe-corrector and Super-X EDX detectors. Observations were performed at 300 kV with a probe convergence angle of 24 mrad. The camera length was set at 77 mm and simultaneous STEM imaging was conducted with three detectors: high-angle annular dark-field (HAADF) with collection angles of 98.7-200 mrad, annular dark-field (ADF) with collection angles of 21.5-98.7 mrad, and annular bright-field (ABF) with collection angles of 10.6 - 21.5 mrad. The resulting spatial resolution achieved was approximately 0.08 nm. Geometric Phase Analysis (GPA) was applied on high-resolution images for nanoscale strain measurements in the GMS Gatan software suite. Energy-Dispersive X-ray Spectroscopy (EDX) was applied to identify the chemical composition of the particles. The powder samples were mixed with Epofix glue, and were prepared by mechanical grinding and polishing (Allied MultiPrep). Final thinning was performed by Ar ion

milling with a Fishione Model 1010, and plasma cleaning was applied before the STEM investigations with a Fishione Model 1020.

Supporting Analyses

Particle polytype identification

Figure 1 of the main text details the microcrystals employed for the present work, by highlighting the large variation in the particle size and shape distribution (see Figure 1a of the main text). Furthermore, Fig. 1 (main text) reveals that the microcrystal sample set is composed of both the 4H, 6H and 15R polytypes, by using a combination of CL and micro-Raman spectroscopy to identify and determine the main spectral signatures of the different SiC polytypes that are present in the initial powder. The spectra in Figure 1(b) (main text) correspond to Raman measurements from individual or small agglomerates of particles (few micron size) acquired at room temperature with an UV laser source of 325 nm. We identify the 6H, 15R and 4H polytypes with reported active Raman modes at 149, 172 and 204 cm^{-1} , respectively, with 6H-SiC being the dominant polytype over all measured particles.

The near band edge emission as collected by CL spectroscopy also provides important information regarding the polytype of each particle. Figure 1(c) of the main text shows a SEM micrograph of select particles (top) and their corresponding CL false colour maps (bottom) displaying the spectral range from 1.6 to 3.3 eV. The hyperspectral CL measurements were recorded at 80 K and the spectra of the marked particles in Fig. 1(c) (main text) are shown in Figure 1(d) (main text). Vertical bars at 2.39, 2.98, 3.02 and 3.26 eV in Fig. 1(d) of the main text illustrate the excitonic energy gap (E_{gX}) reported in the literature for the 3C, 15R, 6H and 4H polytypes, respectively. In general, 3C or 4H polytypes can be easily identified because of the dominant luminescence band centred at around 2.0 or 3.0 eV, respectively, and extending up to or close to their corresponding E_{gX} . In contrast, since 15R and 6H polytypes possess similar E_{gX} , an assignment based on the luminescence band extension would be imprecise. However, we observe that 15R particles generally show a narrow peak at 2.98 eV consistent with its E_{gX} .

Supporting Results and discussion

Particle crystal structure

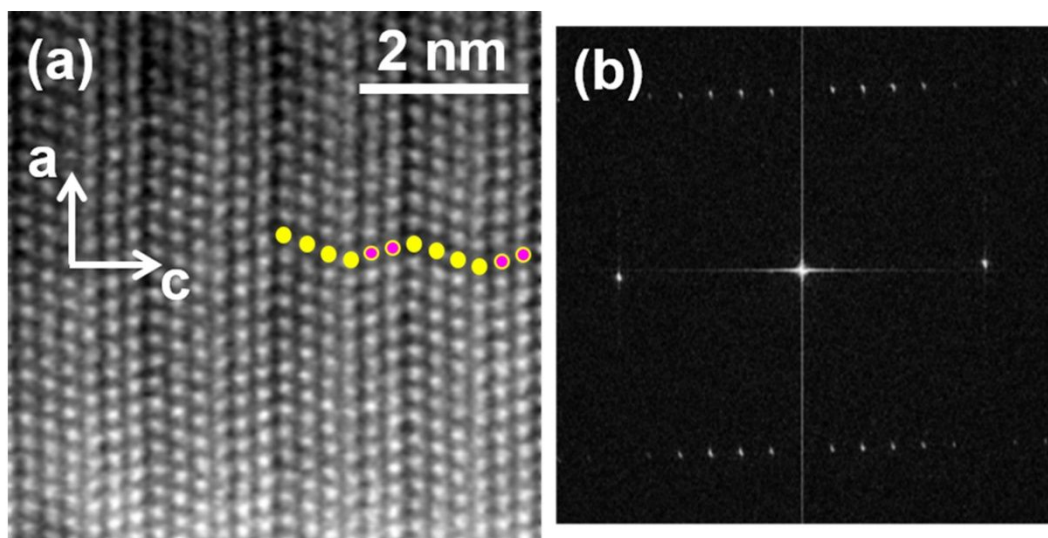


Figure S1. (a) High resolution ADF-STEM image from the edge of the microparticle and (b) fast Fourier transform diffractogram from a larger area, verifying that the particle is of the 6H polytype without other polytype inclusions.

With 6H being identified as the dominant SiC polytype over all studied particles, we now turn to an in-depth investigation of the crystal structure of a representative 6H-SiC microcrystal. Figure S1 illustrates the stacking sequence of a microparticle as collected using scanning transmission electron microscopy, and demonstrates that the particle contains only one polytype. That is, a particle of 6H-SiC polytype will not exhibit polytype inclusions. The characteristic ABCACB stacking sequence of the hexagonal 6H-SiC polytype along the c-axis ([0001] direction) is clearly resolved in Fig. S1. The microparticles were single crystals, and no polytype transformations or extended defects were observed. The fast Fourier transform diffractogram in the inset of Fig. S1 also verifies that the particle is of the 6H polytype without other polytype inclusions.

Distribution of V_{Si} defects after proton irradiation and annealing

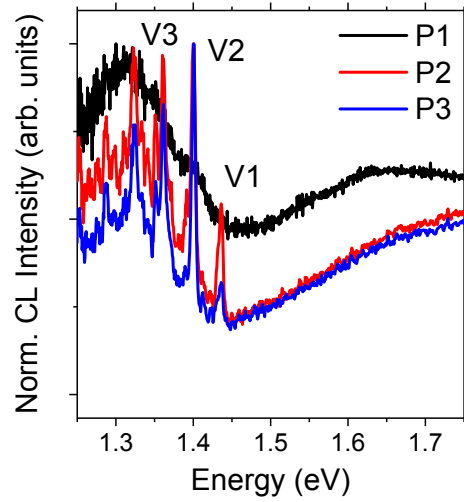


Figure S2. Normalized CL spectra acquired at different localizations within a particle.

Figure S2 shows a normalized version of the CL spectra shown in Fig. 2(e) of the main text from an implanted 6H-SiC particle. V1 is more intense in spot P2 while V2 dominates in P2 over all V_{Si} centers, indicating local changes in the emission efficiency.

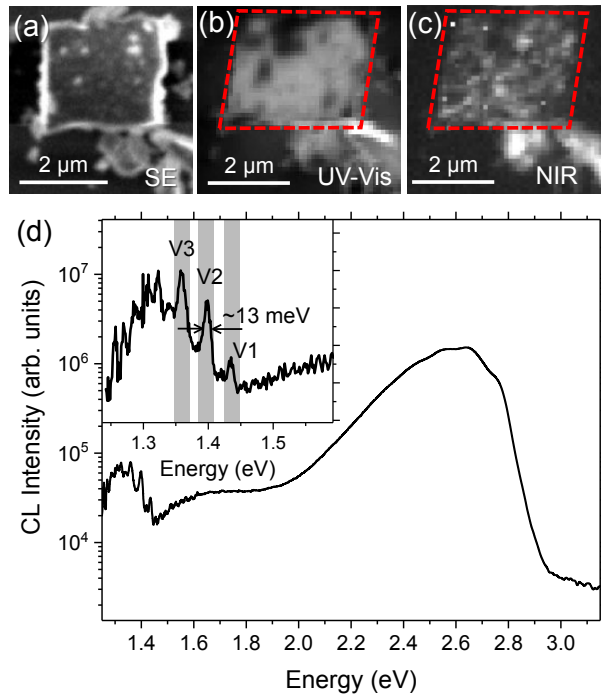


Figure S3. (a) SEM micrograph of a proton-irradiated square particle and its corresponding (b) UV-Visible and (c) NIR intensity maps. The dashed lines in (b) and (c) contour the particle edge. (d) Total CL spectrum at 80 K from the particle in (a). The NIR region has been enlarged in the inset of (d).

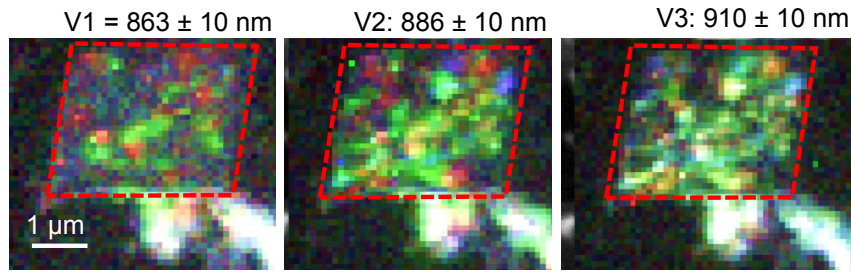


Figure S4. False colour maps demonstrating the distribution of V1, V2 and V3 centres within the proton-irradiated square particle shown in Figure S2, using wavelength windows of 10 nm around the zero phonon line (ZPL).

Next, let us consider the portion of CL emission from the particles that is related to Si vacancies in the 6H SiC polytype. Figure S3(a) shows the SEM micrograph of an irradiated square particle. The particle contour has been marked with a dashed line (note that there is a slight horizontal drift during CL acquisition) in the UV-Vis and NIR CL maps of the Figures S3(b) and S3(c), respectively. The NIR maps present significantly rougher contrast with respect to the UV-Vis map of Fig. S3(b). The CL spectrum acquired from the entire particle is shown in Figure S3(d), with similar characteristics for 6H-SiC as observed the Figure 2(a) of the main text. Details of the NIR region can be observed in the inset of Fig. S3(d), with the V1, V2 and V3 lines peaking at 1.435, 1.399 and 1.359 eV, respectively. Note that the V2 line dominates over V1, and to a lesser extent over V3. Interestingly, the full width at half maximum (FWHM) of V2 and V3 is around 13–14 meV, similar to the FWHM observed averaging over a great number of particles (Figure 2(a) in manuscript). The false colour maps in Figure S4 show the distribution of the different V_{Si} centres embedded within the particle. Note that V3 shows similar distribution as compared to V2.